Journal of Intelligent Material Systems and Structures

Original Article

Journal of Intelligent Material Systems and Structures
2017, Vol. 28(17) 2458–2464

DOI: 10.1177/1045389X17689939
journals.sagepub.com/home/jim
SAGE

Dynamic characterization of elastico-mechanoluminescence towards structural health monitoring

Srivatsava Krishnan, Hugo Van der Walt, Vijay Venkatesh and Vishnu Baba Sundaresan

Abstract

Light emission from zinc sulfide phosphors during elastic loading (elastico-mechanoluminescence, or EML) is characterized for application in structural health monitoring. Micron-sized EML particles are dispersed in an elastomeric matrix for characterization experiments. Numerical models and experimental investigations are combined to arrive at a correlation between EML emission intensity and average stress acting on phosphor particles. A maximum luminance of 25 cd/m^2 is observed from composites with a 6.25:3 phosphor–matrix weight ratio. This intensely bright EML emission is visible under indoor lighting and is attributed to efficient interfacial stress transfer between the matrix and particles facilitated by a moisture-resistant coating. EML emission is captured over 2.5 million actuation cycles and a correlation between the structural health of the elastomer and the measured EML intensity is made. A significant drop in EML emission is observed right before the onset of structural failure which enables real-time prediction and prevention.

Keywords

Elastico-mechanoluminescence, mechanoluminescence, triboluminescence, structural health monitoring, stress visualization, stress sensing, ZnS:Cu

Introduction

Phosphors are multi-functional optical materials that emit light in the visible spectrum from photo, electrical, mechanical, and thermal excitation. The intensity and wavelength of light emitted depends on the phosphor composition, dopant concentration, and excitation energy. Particulate polymer composites embedded with phosphors inherit this optical multi-functional behavior and become self-sensing structures. Among the various modalities, mechanically induced luminescence correlates to structural health and is applicable for continuous health monitoring. Mechanically induced light emission from phosphorescent materials has been gaining widespread attention recently for stress-sensing, stress visualization and crack detection (see, for example, Sage et al., 1999; Sohn et al., 2014; Terasaki and Xu, 2009; Wang et al., 2015; Xu et al., 1999a, and Yun et al., 2013). In particular, recent reports such as Jeong et al. (2013, 2014) on bright light emission from copper doped zinc sulfide micro-particles have been promising owing to durability and repeatability. The phenomenon of mechanoluminescence (ML) has long been known, and in particular, elastico-mechanoluminescence (EML) from doped zinc sulfide materials has been well reported (see, for example, Dickens et al., 2012; Fontenot et al., 2016; Rao et al., 2008; Xu et al., 1999b; Zhang et al., 2012)

Xu et al. (1999a) have studied the EML of thin solid films of ZnS:Mn nanocrystals fabricated by physical vapor deposition techniques on various substrates. Based on their observations of luminance from $^4T_1$–$^6A_1$ transition in the emitting center (Mn) during impact and friction tests, they have explained ML as an interaction of piezoelectricity and electroluminescence. Chandra et al. (2010) have extended this concept with the piezoelectrically induced electron detrapping model for EML of ZnS:Mn. According to this model, straining the non-centrosymmetric crystal of ZnS may produce a local piezoelectric field strong enough to detrap filled electron traps. Energy

Department of Mechanical and Aerospace Engineering, The Ohio State University, USA

Corresponding author:
Vishnu Baba Sundaresan, Department of Mechanical and Aerospace Engineering, The Ohio State University, E528 Scott Lab, 201 W 19th Ave, Columbus, OH 43210, USA.
Email: sundaresan.19@osu.edu

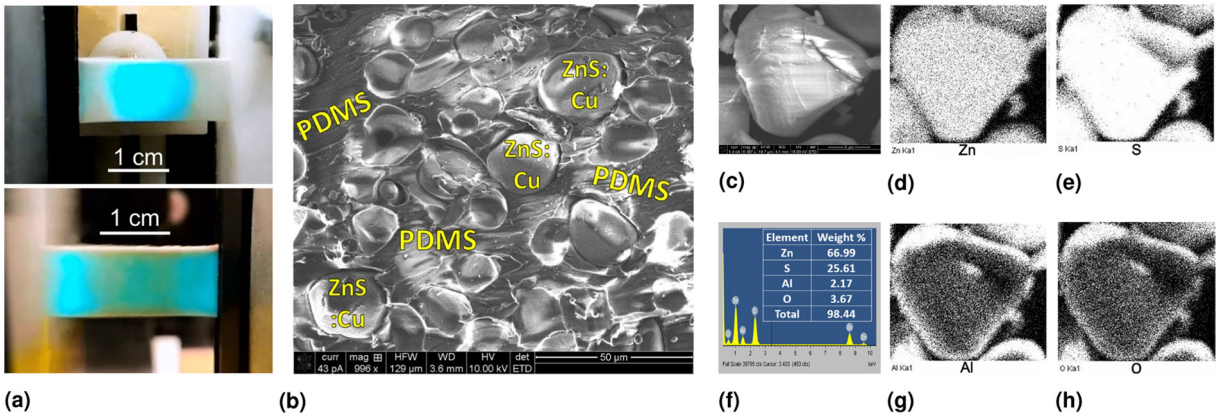

Figure 1. (a) EML from front and back of composite coupon showing stress concentration regions visible under indoor lighting conditions. (b) Scanning electron microscopy (SEM) image of ZnS:Cu–PDMS composite. (c) SEM image of a cut particle. (d) Zinc, (e) sulfur, (g) aluminum, and (h) oxygen elemental maps. (f) Energy Dispersive X-ray spectra and elemental composition.

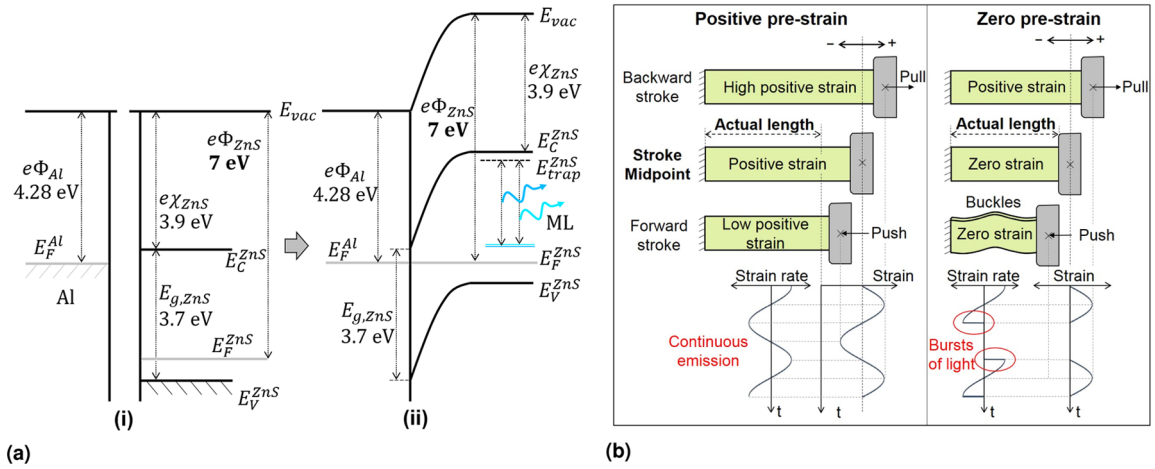

Figure 2. (a) Energy diagram (i) before and (ii) after formation of Al–ZnS:Cu heterojunction; E_F: Fermi level, E_C: conduction band, E_V: valence band, E_{trap}: electron trap level, E_g: band gap, $e\Phi$: work function, $e\chi$: electron affinity. (b) Initial loading conditions of the composite coupons.

from recombination of the detrapped electrons may non-radiatively be transferred to the luminescent ion, inducing excitation and its subsequent de-excitation emits energy in the visible frequency.

ZnS:Cu particles with a moisture-resistant aluminum coating emit intensely bright EML as shown in Figure 1(a). Shin et al. (2015) have suggested that the Al coating acts as an electron source aiding EML emission. However, from the original references cited by the authors, zinc sulfide's work function (7 eV from Fang et al., 2007, and Van Ruyven and Williams, 1966), electron affinity (3.9 eV from Yang et al., 1996), band gap (3.7 eV from Madelung, 2012) and aluminum's work function (4.28 eV from Michaelson, 1977) would yield a heterojunction with a *p*-type depletion region and not a *n*-type accumulation region (Figure 2(a)(ii)). The energy gap between the conduction band and the Fermi levels is about 3.1 eV. Therefore, without external excitation, electron flow from the Fermi level of Al to the conduction band of ZnS, which was hypothesized to make Al an electron source, may not be feasible. Further, the electronic influence of Al coating will be insignificant within the core of the particles and since the particles are 20 μm to 30 μm in size, the majority of the EML emission is expected to be from the crystal bulk. We do believe that the Al coating plays an important role, not electronically, but mechanically, by increasing stress transfer to the EML particles. Experimental evidence and numerical results presented in this work corroborate this belief.

Though the works cited above demonstrate the feasibility of EML for sensing technologies and provide insights into possible origins and mechanisms, a mechanistic understanding of EML is lacking. The

Table 1. EML from various ZnS phosphors under different mechanical loading conditions.

Phosphor	Color	Coating	Crushing	Scribing	Actuation
GL25 [a]	Amber	None	Fracto-ML	EML	No EML
GG13 [b]	Amber	Al-oxide	Fracto-ML	EML	EML
GG25 [b]	Green	Al-oxide	Fracto-ML	EML	EML
GG45 [b]	Blue-green	Al-oxide	Fracto-ML	EML	EML

EML: elastico-mechanoluminescence.
[a]Phosphor Technology Ltd., UK
[b]GTP Corp., USA

motivation of this work is to link the theoretical models developed for EML with the mechanical input parameters such as stress/strain and stress/strain rate towards utilization of EML for structural health monitoring applications in particular. An EML-based structural health monitoring system can address the limitations of current technologies by offering real-time, in situ, distributed sensing and damage detection capabilities.

Experimental methods

Composite coupons of polydimethylsiloxane (PDMS) matrix and EML filler particles were fabricated as outlined in the supporting information. Copper and manganese doped zinc sulfide phosphors (Osram-Sylvania GG-series 45) were used as the EML material due to their intense emission visible in broad daylight.

Composite coupons were observed to emit relatively brighter EML during sudden tugging by hand. Discontinuities in the input load while tugging were reasoned to be the cause of brighter emission. To test this, two initial loading configurations were studied. Figure 2(b) shows the two initial configurations—one with a positive pre-strain and one without. The configuration with positive pre-strain (case I) is actuated with amplitude lower than the pre-strain value ensuring continuous strain/stress curves. The configuration with zero pre-strain (case II) imparts strain/stress only during the positive half of the actuation cycle. The coupon buckles during the negative half-cycle resulting in zero strain/stress and a discontinuous strain input. Luminance measurements were made using a spectroradiometer and temporal studies were carried out with a photoresistor (PR) as shown in Figure 1(b) and 1(c) in the supporting information respectively.

Finite element methods (FEM) were used to predict the stresses experienced by the EML filler particles during longitudinal straining of the composite coupons. Figure 2 in the supporting information shows the FEM model with a particle of elastic ZnS enclosed within a cylindrical volume of hyperelastic PDMS. Supporting information provides more detail on both the experimental setup and FEM model.

Results and discussions

A Scanning electron microscopy (SEM) image of the cross-section of a composite coupon and Energy Dispersive X-ray (EDS) element maps of a fractured EML particle are shown in Figure 1. Element maps reflect the presence of a moisture-resistant aluminum oxyhydroxide coating on the surface of the particles (Fan et al., 2012). The moisture-resistant coating is hydrophobic and binds strongly with the hydrophobic PDMS matrix resulting in better stress transfer and brighter EML emissions. Results from our numerical simulations and lack of EML emission from uncoated phosphors support this belief. Coupons fabricated with GL25 phosphors, which have no coating, did not show EML during elastic actuation, but showed EML when scribed with a glass rod (see Table 1). Scribing the coupon transfers stress directly to the particles, whereas elastic actuation requires efficient stress transfer by the matrix. This strongly emphasizes the importance of aluminum oxyhydroxide coating for stress transfer and EML emission in the GG-series phosphors.

Functional characterization

EML luminance per cycle of actuation, measured from composite coupons with a 7:3 phosphor–PDMS weight ratio, is plotted in Figure 3(a) to (d). Information on the measurement of maximum strains and strain rates is provided in the supporting information.

In case I, a non-linear dependence of EML intensity on the maximum strain rate is observed (Figure 3(a)). At lower strains, practically no EML emission is observed even at moderately high strain rates. The EML emission for 26% strain was detected only by the spectroradiometer and was not visible to the human eye. This establishes the presence of a threshold strain/stress value, below which no visible EML emission occurs. Contrary to case I, EML intensity depends almost linearly on maximum strain rate in case II (Figure 3(b)). Though only half of the actuation cycle induces strain in the coupon, the observed EML intensities are much higher than in case I. Such high intensities, even at low strain rates, are mainly due to the occurrence of two bright bursts of light emission during

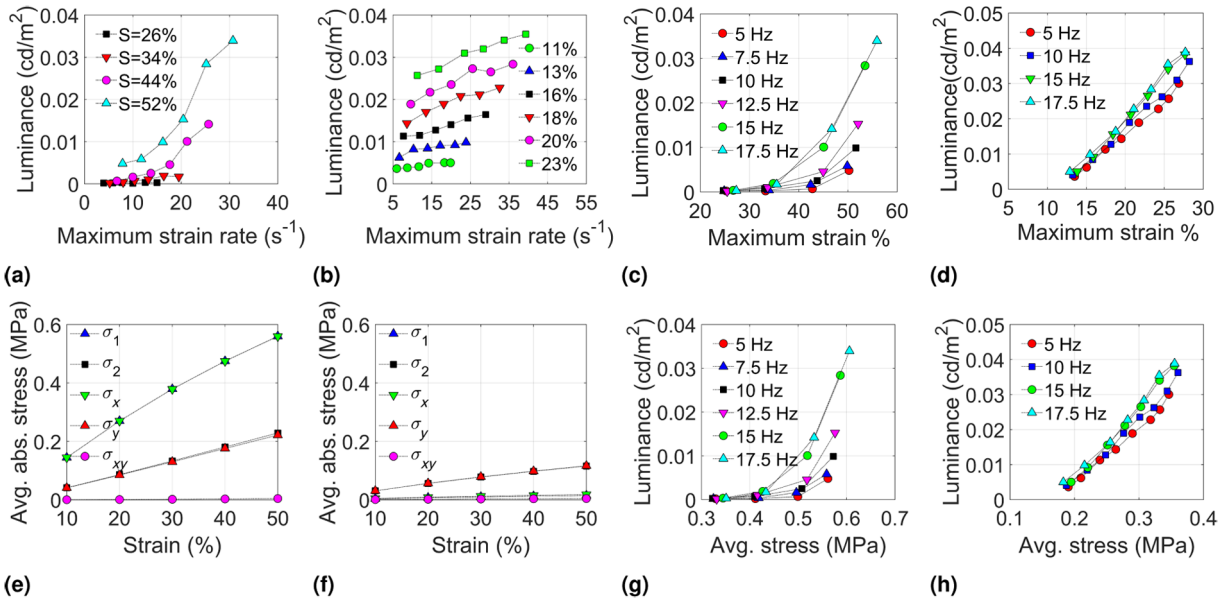

Figure 3. EML dependence on the maximum strain rate for (a) case I and (b) case II. EML dependence on maximum strain (S) for (c) case I and (d) case II. Average absolute stresses (σ) on a particle in (e) complete and (f) zero adhesion with PDMS. EML dependence on average stress for (g) case I and (h) case II.

each cycle that were visibly observed only with case II. Bursts of light emission seem to occur when an abrupt change in strain occurs as shown in Figure 2(b). To establish this, the temporal response of the EML was recorded for both the cases using a photoresistor.

Interfacial stress transfer

Finite element simulations of a ZnS particle in the PDMS matrix were performed to understand the stress transfer from the matrix to the particles. The contact between the particle and matrix was either designed with complete adhesion or zero adhesion to model the maximum and minimum cases of stress transfer respectively. Figure 3(e) and (f) shows the average absolute stresses on the particle in complete and zero adhesion contacts respectively. With complete adhesion, longitudinal tensile stress is transferred efficiently to the particle. This causes the particle to experience average stresses five times higher in magnitude than in the zero adhesion case. This directly indicates the importance of interfacial binding and the selection of a compatible hydrophobic matrix. As mentioned in the previous sections, aluminum coating on the particles forms a strong adhesive bond with the PDMS resembling the complete adhesion case modeled here. Absence of a hydrophobic coating can therefore cripple stress transfer and EML emission significantly, as experimentally observed with GL25 phosphors as well.

Also, from these results, wear and tear of the contact can be expected to reduce interfacial binding, the stress transfer efficiency, and the EML intensity significantly. This is also experimentally observed in the long duration temporal study. Further, combining the characterization data with the numerical solution for complete adhesion, we obtain Figure 3(g) and (h) describing the dependence of EML luminance on the average stress experienced by the EML particles. This is the first effort to characterize EML intensity by average stress on the micron-sized ZnS:Cu particles.

Dependence on weight fraction

Estimating the optimum weight composition of the composites is essential for fabrication of stress-visualizing paints and structural health monitoring sensors. The luminance from coupons with varying phosphor-PDMS weight ratios were longitudinally actuated at 17.5 Hz under a zero pre-strain condition and characterized as mentioned above. The luminance variation with strain is shown in Figure 4. The existence of an optimum weight ratio of 6.25:3 can be explained by identifying two competing factors. With increase in phosphor content, the number of light-emitting sources increases, but particle density within the matrix becomes very high. We believe this results in partial wetting of the particle surface and decreased stress transfer. The proportion of particles emitting light will also be lower at higher compositions.

Short-range temporal response

Figure 5(a) and (b) shows the growth and decay of EML from coupons actuated in cases I and II

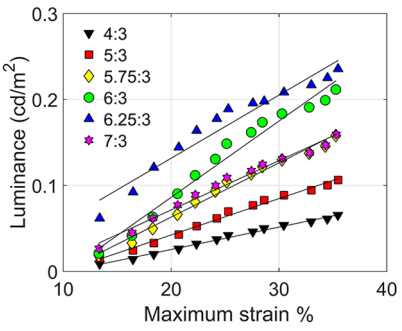

Figure 4. EML luminance variation with coupon composition.

respectively. The black and blue trend lines represent the time-synchronized and scale-adjusted strain and strain-rate curves. Two EML intensity peaks occur in each cycle of actuation, one corresponding to increase and one to decrease in strain/stress. This suggests that EML emission is a dynamic process that requires time-varying strain/stress in crystals. Further, comparing cases I and II, it is evident that the discontinuities in strain and strain-rate curves inherent in case II cause shorter peak rise times as well as higher peak intensities. The sharper and higher intensity peaks are visually observed as bursts of light emission from the coupons as mentioned earlier. Hence, we conclude that higher rate of change of strain causes more de-trapping of electron traps and subsequently brighter EML emission.

Additionally, in both cases, the emission peak due to increase in strain is brighter than the emission peak due to decrease in strain. This is explained by the following hypothesis: the number of filled electron traps available for de-trapping is inversely proportional to the strain state of the crystal at that time instant. The strain at the start of the second peak is higher than that at the start of the first peak. Following this observation, we hypothesize that fewer filled traps are available at the start of the second peak. This directly implies fewer emitted photons and lower EML intensity. Returning to the unstrained state may refill all or most of the electron traps which then become available for the next cycle. This also explains consistent intensities over thousands of actuation cycles for ZnS-based phosphors. Strontium-aluminate-based phosphors do not show this self-recovery behavior which explains the eventual intensity decay with prolonged actuation and intensity increase after short exposure to ultraviolet light (see Chandra et al., 2013). Ultraviolet light excites electrons from the valence band and refills the empty traps which may then become available for EML emission.

Long-range temporal response and failure prediction

Utilizing EML for structural health monitoring applications requires an understanding of the EML response over prolonged cyclic loading. A freshly prepared coupon was actuated at constant amplitude and frequency (25% strain at 20 Hz) and EML emission was tracked by a photoresistor at a 2 Hz sampling rate. Figure 6 shows the EML response over 2.7 million cycles of actuation. The EML intensity increases rapidly at the start, reaches a maximum at around one million cycles, and then decreases linearly until the coupon fails after 2.7 million cycles. This trend can be explained as follows. The polymer chains in a freshly cured coupon are rigid and the coupon is relatively stiff. Stresses within the fresh coupon are therefore concentrated near the ends. As the coupon is cyclically actuated, the rigidity of the polymer chains decreases and stresses are propagated throughout the coupon thereby causing emission from more EML particles. This can be corroborated by images captured at different instances over the loading period.

Also, repetitive actuation may induce wear and tear within the polymer, causing a reduction in interfacial binding between the EML particles and the polymer. Our FEM results suggest that a decrease in interfacial binding causes a significant decrease in stress transfer and EML intensity over time. These two competing factors characterize the EML intensity response observed. Hence, we conclude that EML intensity can be directly

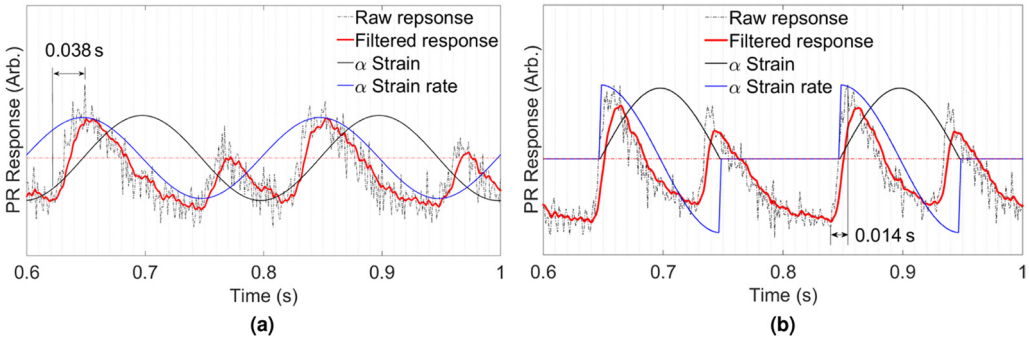

Figure 5. EML temporal response, in terms of photoresistor (PR) response in arbitrary units, for (a) case I and (b) case II.

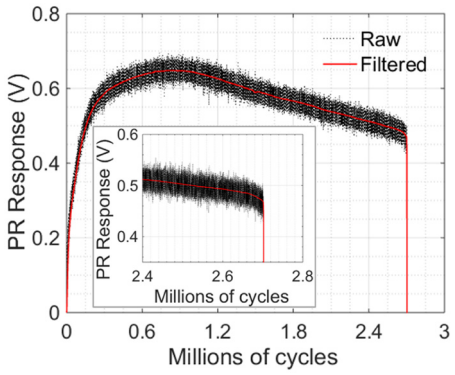

Figure 6. Long-range temporal response. Inset: photoresistor response during failure (black dotted: raw data; red: filtered).

correlated to the structural health of the polymer coupon. Further, the inset of Figure 6 shows the EML intensity decrease significantly right before failure of the coupon, facilitating real-time prediction of impending failure. Though the cycle life varied from coupon to coupon, we consistently observed significant decrease in EML intensity whenever failure occurred. Additional work on benchmarking the first- and second-order time derivatives of EML intensity as failure criteria for real-time prediction is ongoing.

Summary

In this article, we have characterized bright EML emission from composite coupons as a function of input mechanical parameters such as strain/stress and strain rate using experimental and numerical techniques. We have established the highly dynamic behavior of the EML phenomenon, the existence of a threshold strain/stress value and the non-linear dependence on strain and strain rate. The temporal response of EML from composite coupons has also been studied for the first time. Correlation of the EML temporal response with mechanical parameters suggests that discontinuities in the input load cause sharp intense bursts of EML emission. A hypothesis linking the number of filled electron traps in the crystals inversely to the strain in the crystal has also been put forth. This hypothesis explains the lower intensity of EML emissions during decrease in stress than during increase in stress. Over millions of actuation cycles, the EML response has been demonstrated to reflect on the structural health of the polymer coupon. The relaxation of polymer chains leading to more uniform stress distribution and the degradation of interfacial binding due to wear and tear have been captured through the EML response. A methodology for real-time prediction of failure using the EML response has also been outlined in this work, further strengthening the case for an EML-based structural health monitoring technology for composite materials.

Acknowledgements

The authors would like to thank the technical guidance offered by Mr. Duane Detwiler and Ms. Nichole Verwys of Honda R&D Americas.

Declaration of conflicting interests

The author(s) declare no potential conflicts of interest with respect to the research, authorship, and/or publication of this article.

Funding

The author(s) disclosed receipt of the following financial support for the research, authorship, and/or publication of this article: The author(s) would like to acknowledge and thank Honda R&D Americas Ltd. and the NSF-I/UCRC Smart Vehicle Concept Center for financial support.

References

Chandra B, Xu C, Yamada H, et al. (2010) Luminescence induced by elastic deformation of ZnS:Mn nanoparticles. *Journal of Luminescence* 130(3): 442–450.

Chandra V, Chandra B and Jha P (2013) Strong luminescence induced by elastic deformation of piezoelectric crystals. *Applied Physics Letters* 102(24): 241105.

Dickens T, Breaux J, Olawale D, et al. (2012) Effects of ZnS:Mn concentrated vinyl ester matrices under flexural loading on the triboluminescent yield. *Journal of Luminescence* 132(7): 1714–1719.

Fan C, Dang T, Coveleskie J, et al. (2012) *Moisture resistant electroluminescent phosphor with high initial brightness and method of making*. Patent US8298666 B2, USA.

Fang X, Bando Y, Shen G, et al. (2007) Ultrafine ZnS nanobelts as field emitters. *Advanced Materials* 19(18): 2593–2596.

Fontenot RS, Allison SW, Lynch KJ, et al. (2016) Mechanical, spectral, and luminescence properties of ZnS:Mn doped PDMS. *Journal of Luminescence* 170: 194–199.

Jeong SM, Song S, Joo KI, et al. (2014) Bright, wind-driven white mechanoluminescence from zinc sulphide microparticles embedded in a polydimethylsiloxane elastomer. *Energy & Environmental Science* 7(10): 3338–3346.

Jeong SM, Song S, Lee SK, et al. (2013) Mechanically driven light-generator with high durability. *Applied Physics Letters* 102(5): 051110.

Madelung O (2012) *Semiconductors: Data Handbook*. New York, NY: Springer Science & Business Media.

Michaelson HB (1977) The work function of the elements and its periodicity. *Journal of Applied Physics* 48(11): 4729–4733.

Rao NM, Reddy DR, Reddy B, et al. (2008) Intense red mechanoluminescence from $(ZnS)_{1-x}(MNTE)_x$. *Physics Letters A* 372(22): 4122–4126.

Sage I, Badcock R, Humberstone L, et al. (1999) Triboluminescent damage sensors. *Smart Materials and Structures* 8(4): 504.

Shin SW, Oh JP, Hong CW, et al. (2015) Origin of mechanoluminescence from Cu-doped ZnS particles embedded in an elastomer film and its application in flexible electromechanoluminescent lighting devices. *ACS Applied Materials & Interfaces* 8(2): 1098–1103.

Sohn KS, Park WB, Timilsina S, et al. (2014) Mechanoluminescence of $SrAl_2O_4$: Eu^{2+}, Dy^{3+} under cyclic loading. *Optics Letters* 39(6): 1410–1413.

Terasaki N and Xu CN (2009) Mechanoluminescence recording device integrated with photosensitive material and europium-doped $SrAl_2O_4$. *Japanese Journal of Applied Physics* 48(4S): 04C150.

Van Ruyven L and Williams F (1966) Valence-band bending to the Fermi level and radiative recombination in ZnS with liquid electrodes. *Physical Review Letters* 16(20): 889.

Wang X, Zhang H, Yu R, et al. (2015) Dynamic pressure mapping of personalized handwriting by a flexible sensor matrix based on the mechanoluminescence process. *Advanced Materials* 27(14): 2324–2331.

Xu C, Watanabe T, Akiyama M, et al. (1999a) Artificial skin to sense mechanical stress by visible light emission. *Applied Physics Letters* 74(9): 1236–1238.

Xu C, Watanabe T, Akiyama M, et al. (1999b) Preparation and characteristics of highly triboluminescent ZnS film. *Materials Research Bulletin* 34(10): 1491–1500.

Yang Y, Xue S, Liu S, et al. (1996) Fabrication and characteristics of ZnS nanocrystals/polymer composite doped with tetraphenylbenzidine single layer structure light-emitting diode. *Applied Physics Letters* 69(3): 377–379.

Yun GJ, Rahimi MR, Gandomi AH, et al. (2013) Stress sensing performance using mechanoluminescence of $SrAl_2O_4$:Eu (SAOE) and $SrAl_2O_4$:Eu, Dy (SAOED) under mechanical loadings. *Smart Materials and Structures* 22(5): 055006.

Zhang Y, Gao G, Chan HL, et al. (2012) Piezo-phototronic effect-induced dual-mode light and ultrasound emissions from ZnS:Mn/PMN–PT thin-film structures. *Advanced Materials* 24(13): 1729–1735.